Journal of Enhanced Heat Transfer, 25(4-5):367–386 (2018)

UNSTEADY MAGNETOHYDRODYNAMIC CHANNEL FLOW WITH HALL AND ION-SLIP EFFECTS: THE INTEGRAL TRANSFORM SOLUTION PROCEDURE

Bruno N.M. da Silva,[1] Gustavo E. Assad,[2] & João A. de Lima[3,*]

[1]*Post-Graduate Program of Mechanical Engineering, UFRN, Natal-RN, Brazil*

[2]*Federal Institute of Technology, IF/PB, João Pessoa-PB, Brazil*

[3]*Renewable Energy Engineering Department, UFPB/CEAR, João Pessoa-PB Brazil*

*Address all correspondence to: João A. de Lima, Renewable Energy Engineering Department, UFPB/CEAR, João Pessoa-PB Brazil; Tel./Fax: +55 83 3216 7268, E-mail: jalima@cear.ufpb.br

Original Manuscript Submitted: 10/17/2017; Final Draft Received: 3/11/2018

This paper deals with the generalized integral transform solution procedure to the unsteady magneto-convection problem of an electrically conducting Newtonian fluid within a parallel-plate channel, in which Hall and ion-slip effects are taken into account. It is considered that the magnetic Reynolds number is small, i.e., the flow-induced magnetic fields are not strong enough to modify the applied transversal magnetic field. To cover a broader range of problems, temperature-dependent transport properties, time-dependent pressure gradient, inflow perpendicular to the plates (porous plates), and Couette flow are also considered in the mathematical formulation. Results are illustrated and compared to the main numerical results from the literature for the related velocity and temperature potentials as function of the main governing parameters, namely, Hartmann, suction/injection, transport properties, and electron and ion-slip parameters. In order to illustrate the consistency of the Generalized Integral Transform Technique (GITT) and its use for benchmarking purposes in the magneto fluid dynamics area, convergence analyses are carried out for the main potentials.

KEY WORDS: *magnetohydrodynamics, magneto-convection, Hall and ion-slip effects, integral transforms, channel flow*

1. INTRODUCTION

Appearing in the early twentieth century, interest in magnetohydrodynamics (MHD) came back in the 1960s, and currently, is the subject of several experimental and computational investigations. MHD is present in a number of areas, from geophysics to nuclear engineering to metallurgical and materials engineering. An increasing number of engineering applications makes use of MHD to control, suppress, drive, and generate motion in several devices through electrically conducting fluids (Shercliff, 1965; Davidson, 2001; Sutton and Sherman, 2006). Inside of some

of these devices, flows in parallel-plate passages are normally present, being the geometric configuration that is usually employed by computational approaches for "benchmarking" purposes.

Normally, in the computational approach, additional features that impose some degree of numerical difficulty are gradually added to a basic situation, thus requiring more insight on the physical, mathematical, and numerical aspects of MHD modeling and solution. For example, the steady-state fully developed generalized MHD Couette flow with heat transfer was studied by Attia and Kotb (1996). Plate porosities and temperature-dependent fluid viscosity were also included in the analysis. Later on, by neglecting the plate porosities, but considering that all transport properties (viscosity, thermal, and electrical conductivities) were temperature-dependent, Attia (2006a) extended that previous study. Hall and ion-slip effects were firstly introduced by Attia (2003) when analyzing the steady-state fully developed MHD plane-Poiseuille flow.

The unsteady-state regime was considered by Attia (1999), who studied the transient MHD plane-Poiseuille flow with heat transfer under a temperature-varying viscosity. Later, the problem was extended to incorporate the Hall effect (Attia, 2005a), and the Hall effect and temperature dependency for all transport properties (Attia and Aboul-Hassan, 2003). The simultaneous effects of Hall and ion slip were analyzed by Attia (2006b) in a work that considered constant transport properties and brought back the hypothesis of porous plates. Additionally, the author considered that the flow field was driven by an exponentially decaying pressure gradient. Unsteady Couette flow with heat transfer and variable properties and Hall effects was then studied by Attia (2008a).

Extensions of these studies for dusty flows with particles in suspension (such as ash or soot) were performed by Attia (2002, 2005b,c, 2006c, 2008b), and Attia et al. (2016), among others.

The fact that all the cited studies employed some sort of numerical method, or approximate approaches such as the regular perturbation method, to solve the governing equations must be observed. Although it is not the case for the problems above referenced, solution procedures to the multi-physic MHD equations (the Navier–Stokes and the MHD-electrodynamics' equations) normally face some numerical or limiting problems related to the strong coupling between the flow and the magnetic equations, and the non-linear nature of these equations. Hybrid methods such as the so-called Generalized Integral Transform Technique (GITT) have been employed to solve heat and fluid-flow problems with relative success. GITT is a numerical–analytical method that keeps all the characteristics of an analytical solution (similar to the method of separation of variables), combined with the robustness of the purely numerical methods for solution of systems of ordinary differential equations (when solving systems of partial differential equations). By exploiting their automatic local and global error control, this technique is a reliable alternative for obtaining benchmark results for convection–diffusion problems, as it has been demonstrated along the years (Ozisik and Murray, 1974; Mikhailov and Ozisik, 1984; Cotta, 1993, 1998; Cotta and Mikhailov, 1997; Cotta et al., 2013; Santos et al., 2001; Castelloes and Cotta, 2006; Naveira et al., 2009).

Regarding the MHD forced convection, performance of the integral transform method can be assessed in the work of Lima et al. (2007), who analyzed the same problems studied by Attia and Kotb (1996) and Attia (1999), and in the work of Lima and Rêgo (2013), who studied the steady-state simultaneously developing force convection in the entrance region of a parallel-plate channel using a boundary layer formulation, and compared their results with the numerical results of Shohet et al. (1962), Hwang et al. (1966), and Setayesh and Sahai (1990) for different physical situations. More recently, Pontes et al. (2017) solved the Navier–Stokes version of the problem studied by Lima and Rêgo (2013), and Matt et al. (2017) solved the MHD natural convection of an electrically conducting fluid within a square cavity, differentially heated at the

sidewalls and subjected to an inclined magnetic field. One year before, the generalized integral transform method was employed by Assad (2016) to analyze the mutual interaction between the flow and the magnetic fields in the entrance region of a parallel-plate channel, by solving the coupled system represented by the Navier–Stokes and the magnetic field equations (using the stream-function formulation for the flow field, and a scalar magnetic potential for the magnetic field).

Therefore, the main goal of the present work is to extend the range of physical problems that can be handled with the integral transform method, showing its outstanding characteristics for benchmark purposing. Specifically, this is attained by illustrating convergence analyses and comparing results for the unsteady Hartmann plane-Poiseuille or Couette flow with Hall and ion-slip effects with other numerical findings for the main potentials, as function of the governing parameters, namely, Hartmann, suction/injection, and electron and ion-slip parameters. It must be clear that despite accounting for Hall and ion-slip effects, it is still considered that the electric currents induced in the flow field are not strong enough to alter the applied external magnetic field, i.e., the hypothesis of small magnetic Reynolds number is adopted ($\mathrm{Re}_m \ll 1$).

To cover a broader range of physical situations, a formulation is used in which fluid suction/ejection through the channel walls, exponentially varying pressure gradient as well as temperature-dependent transport properties can occur. All the mentioned physical effects can be analyzed simultaneously or can be studied in a separated or combined form to a particular application, depending on the values used for the governing dimensionless parameters.

2. MATHEMATICAL FORMULATION

By considering a rectangular channel in which the two horizontal plates are electrically insulated (porous or not) separated by a distance h, kept at constant temperatures (different or not), and the two vertical plates are electrical conductors (to which a resistive load/electrical source can be connected), the governing equations (and the corresponding initial and boundary conditions) are written in dimensionless form as

$$\frac{\partial u}{\partial t} + R_v \frac{\partial u}{\partial y} = -\frac{\partial P}{\partial x} + \frac{\partial}{\partial y}\left(\mu\left[T\right]\frac{\partial u}{\partial y}\right) - \frac{\mathrm{Ha}^2 \sigma\left[T\right]}{\left(1+\beta_e\beta_i\right)^2+\beta_e^2}\left[\left(1+\beta_e\beta_i\right)\left(E_z+u\right)+\beta_e w\right] \tag{1}$$

$$\frac{\partial w}{\partial t} + R_v \frac{\partial w}{\partial y} = \frac{\partial}{\partial y}\left(\mu\left[T\right]\frac{\partial w}{\partial y}\right) - \frac{\mathrm{Ha}^2 \sigma\left[T\right]}{\left(1+\beta_e\beta_i\right)^2+\beta_e^2}\left[\left(1+\beta_e\beta_i\right) w - \beta_e\left(E_z+u\right)\right] \tag{2}$$

$$\frac{\partial T}{\partial t} + R_v \frac{\partial T}{\partial y} = \frac{1}{\mathrm{Pr}}\frac{\partial}{\partial y}\left(k\left[T\right]\frac{\partial T}{\partial y}\right) + \mathrm{Ec}\mu\left[T\right]\left\{\left(\frac{\partial u}{\partial y}\right)^2 + \left(\frac{\partial w}{\partial y}\right)^2\right\} + \frac{\mathrm{Ec}\,\mathrm{Ha}^2 \sigma\left[T\right]}{\left(1+\beta_e\beta_i\right)^2+\beta_e^2}\left[\left(E_z+u\right)^2 + w^2\right] \tag{3}$$

$$u\left(y,0\right)=0, \quad w\left(y,0\right)=0, \quad T\left(y,0\right)=0\}; \quad t=0, \quad 0<y<1 \tag{4}$$

$$u\left(0,t\right)=0, \quad w\left(0,t\right)=0, \quad T\left(0,t\right)=0\}; \quad y=0, \quad t>0 \tag{5}$$

$$u\left(1,t\right)=R_u, \quad w\left(1,t\right)=0, \quad T\left(1,t\right)=1\}; \quad y=1, \quad t>0 \tag{6}$$

The following dimensionless groups were adopted in the above equations:

$$x = \frac{x^*}{h}, \quad y = \frac{y^*}{h}, \quad u = \frac{u^* h}{\nu_1^*}, \quad w = \frac{w^* h}{\nu_1^*}, \quad t = \frac{t^* \nu_1^*}{h^2}, \quad \mu = \frac{\mu^*}{\mu_1^*}, \quad k = \frac{k^*}{k_1^*},$$
$$\sigma = \frac{\sigma^*}{\sigma_1^*}, \quad \mathrm{Pr} = \frac{k_1^*}{\mu_1^* c_p}, \quad R_u = \frac{u_2^* h}{\nu_1^*}, \quad R_v = \frac{v_0^* h}{\nu_1^*}, \quad P = \frac{h^2 P^*}{\rho \nu_1^{*2}}, \quad T = \frac{T^* - T_1^*}{T_2^* - T_1^*}, \tag{7}$$
$$\mathrm{Ec} = \frac{\nu_1^{*2}}{h^2 c_p \left(T_2^* - T_1^*\right)}, \quad E_z = \frac{h}{\nu_1^*} \frac{E_0}{B_0}, \quad \mathrm{Ha} = B_0 h \sqrt{\frac{\sigma_1^*}{\mu_1^*}}$$

In these groups, u and w are the dimensionless longitudinal and the induced transversal (due to Hall and ion-slip effects) velocity components. T is the dimensionless temperature. Ha, Pr, and Ec stand for Hartmann, Prandtl, and Eckert numbers, and β_e and β_i, in the last terms of the governing equations are the Hall and ion-slip parameters, respectively. R_u and R_v are the dimensionless upper-wall and wall suction/ejection velocities, respectively. Flow can be sustained by a constant or a time-decaying pressure gradient, and since the magnetic Reynolds number is considered small ($\mathrm{Re}_m = \mu_{m1}^* \sigma_1^* h\, u^* \ll 1$), there is no induced magnetic field. Indices 1 and 2 refer to properties evaluated at the bottom-wall and upper-wall temperatures, respectively.

The pressure gradient and the transport properties are given as follows:

$$\frac{\partial P}{\partial x}(t) = G_0 \left(e^{-i_{\alpha G}\, \alpha_G t} \right) \tag{8a}$$

$$\mu(T) = e^{-a\,T} \tag{8b}$$

$$k(T) = 1 + b\,T \tag{8c}$$

$$\sigma(T) = 1 + c\,T \tag{8d}$$

G_0 is the constant pressure gradient and $i_{\alpha G}$ is a flag parameter that indicates if the pressure gradient is a function of time ($i_{\alpha G} = 1$) or not ($i_{\alpha G} = 0$), α_G being the time-decaying factor. Now, since the boundary conditions do not depend on the x coordinate, the problem has a fully developed solution of the form

$$u \equiv u\,(y, t) \tag{8e}$$

$$v \equiv R_v \tag{8f}$$

$$w \equiv w\,(y, t) \tag{8g}$$

$$P \equiv P_0 + G_0 \left(e^{-i_{\alpha G}\, \alpha_G t} \right) x \tag{8h}$$

Then, the continuity equation, $(\partial u/\partial x) + (\partial v/\partial y) + \partial w/\partial z = 0$, is automatically satisfied.

3. INTEGRAL TRANSFORM SOLUTION PROCEDURE

3.1 Splitting Up of Potentials

To take full advantage of its hybrid nature, the integral transform method requires that the boundary conditions in the direction to be integral transformed to be homogeneous. Since the boundary conditions at the upper plate are inhomogeneous, the following splitting up of the longitudinal velocity component and temperature is proposed:

$$u(y, t) = u_h(y, t) + u_F(y) \tag{9a}$$

$$T(y,t) = T_h(y,t) + T_F(y) \tag{9b}$$

$u_h(y,t)$ and $T_h(y,t)$ are the homogenized (the filtered) potentials. As long as the inhomogeneities are taken into account, any expressions for the filtering solutions, $u_F(y)$ and $T_F(y)$, can be employed. However, it is advisable to use expressions that carry as much information as possible about the problem being solved. Therefore, for the flow field, we choose the steady-state, constant-properties, and constant-pressure gradient, fully developed MHD-flow expression, with no Hall nor ion-slip effects. For the temperature field, only the diffusion phenomenon was considered. Then, the following equations were considered for filtering purposes:

$$0 = -G_0\,(1 - i_{\alpha G}) + \frac{d^2u_F}{dy^2} - \mathrm{Ha}^2(E_z + u_F), \quad \begin{cases} u_F(0) = 0 \\ u_F(1) = R_u \end{cases} \tag{10}$$

$$0 = \frac{d^2T_F}{dy^2}, \quad \begin{cases} T_F(0) = 0 \\ T_F(1) = 1 \end{cases} \tag{11}$$

Their solutions are easily obtained as [with $G_G = G_0\ (1 - i_{\alpha G}) + \mathrm{Ha}^2 E_z$]

$$u_F(y) = \begin{cases} \Big\{G_G\,(1 - \cosh\left[\mathrm{Ha}\,y\right]) + \left\{G_G\,(\cosh\left[\mathrm{Ha}\right] - 1) + \mathrm{Ha}^2 R_u\right\} \\ \qquad\qquad \times \left[(\sinh\left[\mathrm{Ha}\,y\right])/(\sinh\left[\mathrm{Ha}\right])\right]\Big\}/\mathrm{Ha}^2, & \mathrm{Ha} \neq 0 \\ \dfrac{G_G}{2}\left(y - y^2\right) + R_u\,y, & \mathrm{Ha} = 0 \end{cases} \tag{12}$$

$$T_F(y) = y \tag{13}$$

This procedure automatically guarantees the GITT requirements of homogeneity of boundary conditions and, additionally, reduces the convergence needing as the fully developed (MHD or non-MHD) steady-state regime is approaching.

3.2 Integral Transformation

After the splitting-up procedure the equations must be integral transformed using the eigenfunctions and the orthogonality properties associated to appropriate eigenvalue problems. The following eigenvalue problem was adopted to all potentials:

$$\frac{d^2\tilde{\psi}_i(y)}{dy^2} = -\lambda_i^2\,\tilde{\psi}_i(y), \quad \begin{cases} \tilde{\psi}_i(0) = 0 \\ \tilde{\psi}_i(1) = 0 \end{cases} \tag{14}$$

This eigenvalue problem has the following properties:

$$\psi_i(y) = \frac{\tilde{\psi}_i(y)}{N_i^{1/2}} = \sqrt{2}\sin(\lambda_i y),$$

$$\begin{cases} \lambda_i = i\pi, & i = 1, 2, 3, ... \\ \int_0^1 \tilde{\psi}_i(y)\,\tilde{\psi}_j(y)\,dy = \begin{cases} 0, & i \neq j \\ N_i = 1/2, & i = j \end{cases} \end{cases} \tag{15}$$

Then, the following integral transform/inverse pairs for velocity and temperature fields are proposed:

$$\left\{\begin{array}{l} u_h(y,t)=\sum\limits_{i=1}^{\infty}\psi_i(y)\,\bar{u}_{hi}(t) \\ \bar{u}_{hi}(t)=\int_0^1\psi_i(y)\,u_h(y,t)\,dy \end{array}\right. , \quad \left\{\begin{array}{l} w(y,t)=\sum\limits_{i=1}^{\infty}\psi_i(y)\,\bar{w}_i(t) \\ \bar{w}_i(t)=\int_0^1\psi_i(y)\,w(y,t)\,dy \end{array}\right. ,$$
$$\left\{\begin{array}{l} T_h(y,t)=\sum\limits_{i=1}^{\infty}\psi_i(y)\,\bar{T}_{hi}(t) \\ \bar{T}_{hi}(t)=\int_0^1\psi_i(y)\,T_h(y,t)\,dy \end{array}\right. \tag{16}$$

To be integral transformed, the homogenized versions of the governing equations are firstly multiplied by the eigenfunctions and then integrated over the domain [$\int_0^1\psi_i(y)$ (Eqs.) dy], resulting in the following transformed system of coupled ordinary differential equations with the respective transformed initial conditions:

$$\frac{d\bar{u}_{hi}(t)}{dt}=G_0\bar{f}_i\left(e^{-i_{\alpha G}\alpha_G t}\right)+\bar{B}_{ui},\quad i=1,2,3,...,\infty \tag{17a}$$

$$\bar{u}_{hi}(0)=-\bar{h}_i,\quad i=1,2,3,...,\infty \tag{17b}$$

$$\frac{d\bar{w}_i(t)}{dt}=\bar{B}_{wi},\quad i=1,2,3,...,\infty \tag{17c}$$

$$\bar{w}_i(0)=0,\quad i=1,2,3,...,\infty \tag{17d}$$

$$\frac{d\bar{T}_{hi}(t)}{dt}=\bar{B}_{Ti},\quad i=1,2,3,...,\infty \tag{17e}$$

$$\bar{T}_{hi}(0)=-\bar{g}_i,\quad i=1,2,3,...,\infty \tag{17f}$$

The transformed coefficients are written as follows:

$$\bar{f}_i=\int_0^1\psi_i(y)dy=-\frac{\sqrt{2}}{\lambda_i}\left[(-1)^i-1\right] \tag{18a}$$

$$\bar{h}_i=\int_0^1\psi_i(y)u_F(y)dy=\frac{\sqrt{2}\left(G_G-(-1)^i\left[G_G+\lambda_i^2R_u\right]\right)}{\lambda_i\left(Ha^{\quad 2}+\lambda_i^2\right)} \tag{18b}$$

$$\bar{g}_i=\int_0^1\psi_i(y)T_F(y)dy=-\frac{\sqrt{2}}{\lambda_i}(-1)^i \tag{18c}$$

$$\begin{aligned}\bar{B}_{ui}=-\int_0^1\Bigg\{&\left(\psi_iR_v+\psi_i'\mu\left[T\right]\right)\frac{\partial u}{\partial y}\\&+\psi_i\frac{\mathrm{Ha}^2\sigma[T]}{\left(1+\beta_i\beta_e\right)^2+\beta_e^2}\left[\left(1+\beta_i\beta_e\right)\left(E_z+u\right)+\beta_ew\right]\Bigg\}dy\end{aligned} \tag{18d}$$

$$\begin{aligned}\bar{B}_{wi}=-\int_0^1\Bigg\{&\left(\psi_iR_v+\psi_i'\mu\left[T\right]\right)\frac{\partial w}{\partial y}\\&+\psi_i\frac{\mathrm{Ha}^2\sigma\left[T\right]}{\left(1+\beta_i\beta_e\right)^2+\beta_e^2}\left[\left(1+\beta_i\beta_e\right)w-\beta_e\left(E_z+u\right)\right]\Bigg\}dy\end{aligned} \tag{18e}$$

$$\bar{B}_{Ti} = -\int_0^1 \left\{ \left(\psi_i R_v + \psi_i' \frac{k\,[T]}{\mathrm{Pr}} \right) \frac{\partial T}{\partial y} + \psi_i \mathrm{Ec} \left\{ \mu\,[T] \left[\left(\frac{\partial u}{\partial y} \right)^2 + \left(\frac{\partial w}{\partial y} \right)^2 \right] + \frac{\mathrm{Ha}^2 \sigma\,[T]}{(1+\beta_i\beta_e)^2 + \beta_e^2} \left[(E_z + u)^2 + w^2 \right] \right\} \right\} dy \tag{18f}$$

3.3 Numerical Solution of the Transformed System

If each eigen-expansion is truncated in a finite number of terms, $NU = NW = NT = N$, then we have a final coupled system of $3N$ first-order ordinary differential equations for the transformed potentials.

To solve this transformed system [the truncated version of Eqs. (17) and (18)], a Fortran 90 code was developed and routine IVPAG from IMSL(2010) was employed with an error target of 10^{-8} as the tolerance criterion. This routine uses the Gear's implicit linear multistep method, which is appropriate to handle stiff systems of initial-value problems. For all results shown, $N = 300$ terms was used on the computations. The non-transformable integral coefficients, Eqs. (18d)–(18f), are dynamically obtained through routine FQRUL (IMSL, 2010) that uses Fejer-quadrature rules for numerical integration. NQR = 10,000 points of quadrature were used in order to guarantee that all coefficients were evaluated within the appropriate accuracy.

4. RESULTS AND DISCUSSION

Results for the longitudinal and transversal velocity components, temperature, longitudinal and transversal skin friction coefficients, and Nusselt number, at the bottom and upper plates are evaluated according to their definition, the relation with the inverse formulae and the filtering expressions, for different combinations of the governing parameters (Ha, G_o, α_G, $i_{\alpha G}$, R_u, R_v, Pr, Ec, E_z, a, b, c, β_e, β_i) as

$$u(y,t) = \sum_{i=1}^{N} \psi_i(y)\bar{u}_{hi}(t) + u_F(y) \tag{19a}$$

$$w(y,t) = \sum_{i=1}^{N} \psi_i(y)\bar{w}_i(t) \tag{19b}$$

$$T(y,t) = \sum_{i=1}^{N} \psi_i(y)\bar{T}_{hi}(t) + T_F(y) \tag{19c}$$

$$\begin{aligned} \tau_{x0} &= \left.\frac{\partial u}{\partial y}\right|_{y=0} = \sum_{i=1}^{N} \psi_i'(0)\bar{u}_{hi}(t) + u_F'(0); \\ \tau_{x1} &= \left.\frac{\partial u}{\partial y}\right|_{y=1} = \sum_{i=1}^{N} \psi_i'(1)\bar{u}_{hi}(t) + u_F'(1) \end{aligned} \tag{20}$$

$$\tau_{y0} = \left.\frac{\partial w}{\partial y}\right|_{y=0} = \sum_{i=1}^{N} \psi_i'(0)\bar{w}_i(t); \quad \tau_{y1} = \left.\frac{\partial w}{\partial y}\right|_{y=1} = \sum_{i=1}^{N} \psi_i'(1)\bar{w}_i(t) \tag{21}$$

$$\begin{aligned} \mathrm{Nu}_0 &= \left.\frac{\partial T}{\partial y}\right|_{y=0} = \sum_{i=1}^{N} \psi_i'(0)\bar{T}_{hi}(t) + T_F'(0); \\ \mathrm{Nu}_1 &= \left.\frac{\partial T}{\partial y}\right|_{y=1} = \sum_{i=1}^{N} \psi_i'(1)\bar{T}_{hi}(t) + T_F'(1) \end{aligned} \tag{22}$$

In the following figures and tables, subscript A stands for variable relative to the reference used for comparisons, most of them due to Attia, who used different characteristic scales for definition of his dimensionless parameters.

Figures 1(a) and 1(b) depict comparisons for the axial velocity profile with the findings of Attia (2006a), for the generalized steady-state Couette flow with temperature-dependent physical properties. Results are compared for Ha = 2 and 6, $G_o = 40$, $\alpha_G = 0$ ($i_{\alpha G} = 0$), $R_u = 2$, $R_v = 0$, Pr = 1, Ec = 0.05, $E_z = 0$, $b = 0$, $\beta_e = 0$, $\beta_i = 0$ and different values of viscosity parameter a, and electrical conductivity parameter c. Additional comparisons for this geometry can be found in the work of Lima et al. (2007), who reproduced the results of Attia and Kotb (1996). Figure 1(a) illustrates the case for $a = -0.5$ and Fig. 1(b) for $a = 0.5$.

These figures show the strong influence of the magnetic field (Hartmann number) and the transport properties parameters (a and c) on the fully developed velocity profile. As expected, an increase in Ha promotes a strong reduction on the velocity field (the retarding Lorentz force effect). This effect is more intensified by decreasing the viscosity parameter (which makes the viscosity increase with temperature) and increasing the electrical conductivity parameter (which makes the electrical conductivity increase with temperature, thus increasing the retarding force).

In Fig. 1(b), despite the differences for the situation ($a = 0.5$, $c = 0$, and Ha $= 2$) being small, the present results do not match the results of Attia (2006a) for ($a = 0.5$, $c = -0{,}5$ and Ha $= 2$). As the problem here studied is quite simple (fully developed flow), it is believed that the results presented by Attia (2006a) contain some numerical error, are not fully converged, or were obtained for a simulation with viscosity and/or electrical parameters different from the present runs.

Table 1 illustrates quantitative comparisons for the centerline temperature for different values of the physical properties (a, b, c), with no Hall or ion-slip effects ($\beta_e = \beta_i = 0$), for Ha $= 2$ and 6. Notice that even for the simplest situation, i.e., constant physical properties ($a = b =$

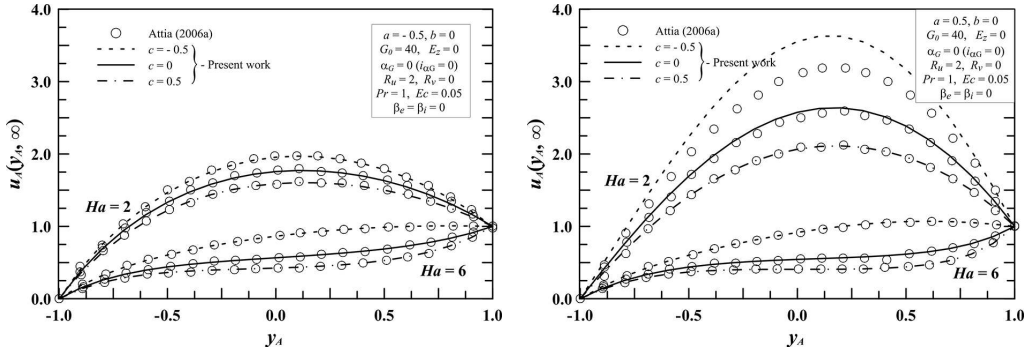

FIG. 1: Axial velocity component profiles for the steady-state MHD Couette flow for different values of Hartmann (Ha) and property parameters (a and c). (a) $a = -0.5$, (b) $a = 0.5$

TABLE 1: Comparisons for the steady-state temperature at the channel centerline for different values of physical properties coefficients (a, b, c) and Hartmann number (Ha)

$T\,(y_A = 0, \infty)$							
		Present	**Attia (2006a)**	**Present**	**Attia (2006a)**	**Present**	**Attia (2006a)**
$b = 0$		$a = -0.5$		$a = 0$		$a = 0.5$	
Ha = 2	$c = -0.5$	0.8779	0.8794	1.0150	1.0134	1.2965	1.2165
	$c = 0$	0.9061	0.9069	1.0320†	1.0333	1.2350	1.2176
	$c = 0.5$	0.9215	0.9217	1.0265	1.0285	1.1655	1.1637
Ha = 6	$c = -0.5$	0.8802	0.8758	0.8883	0.8859	0.9022	0.8963
	$c = 0$	0.8183	0.8155	0.7920†	0.7925	0.7754	0.7752
	$c = 0.5$	0.7769	0.7750	0.7427	0.7442	0.7218	0.7227
$c = 0$		$a = -0.5$		$a = 0$		$a = 0.5$	
Ha = 2	$b = -0.5$	1.0441	1.0334	1.3902	1.2951	1.2965	1.6810
	$b = 0$	0.9061	0.9069	1.0320†	1.0333	1.2350	1.2176
	$b = 0.5$	0.8526	0.8511	0.9374	0.9377	1.0600	1.0555
Ha = 6	$b = -0.5$	0.9000	0.8833	0.8458	0.8393	0.8154	0.8099
	$b = 0$	0.8183	0.8155	0.7920†	0.7925	0.7754	0.7752
	$b = 0.5$	0.7871	0.7827	0.7691	0.7670	0.7575	0.7548
$a = 0$		$b = -0.5$		$b = 0$		$b = 0.5$	
Ha = 2	$c = -0.5$	1.3007	1.2117	1.0158	1.0134	0.9286	0.9282
	$c = 0$	1.3904	1.2951	1.0320†	1.0333	0.9381	0.9377
	$c = 0.5$	1.3609	1.2982	1.0269	1.0285	0.9347	0.9339
Ha = 6	$c = -0.5$	1.0864	1.0138	0.8883	0.8859	0.8331	0.8305
	$c = 0$	0.8458	0.8393	0.7920†	0.7925	0.7691	0.7670
	$c = 0.5$	0.7607	0.7606	0.7427	0.7442	0.7337	0.7322

†Present approach and analytical solution

$c = 0$) for which analytical solutions can be easily obtained, results of Attia (2006a) are not accurate.

Results for the unsteady flow regime with heat transfer considering variable properties and Hall effects are now illustrated and compared to the findings of Attia (2008a) for Couette flow, and of Attia and Aboul-Hassan (2003) and Attia (2005a) for plane-Poiseuille flow.

Figures 2–4 bring comparisons for the velocity components and temperature profiles, for Ha = 2, $G_o = 40$, $\alpha_G = 0$ ($i_{\alpha G} = 0$), $R_v = 0$, Pr = 1, Ec = 0.05, $E_z = 0$, $a = 0.5$, $b = 0.5$, $c = 0$, $\beta_e = 3$, $\beta_i = 0$ at different instants of time, for the generalized Couette ($R_u = 2$) and plane-Poiseuille ($R_u = 0$) flows.

The excellent matching between the present hybrid results and the numerical ones are easily verified. Physically, as expected, the symmetry of the flow field is broken by the moving plate of the Couette configuration. Alterations on the temperature field are very subtle.

To illustrate the direct influence of the applied magnetic field on the flow field, the same set of figures for the velocity components is illustrated in Figs. 5 and 6 for Ha = 6 and Ha = 10.

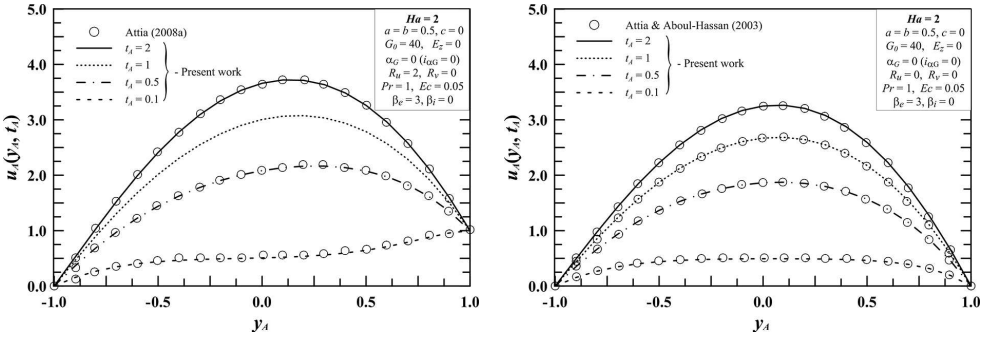

FIG. 2: Axial velocity component profiles for the unsteady MHD: (a) Couette and (b) plane-Poiseuille flow at different times for Ha $= 2$

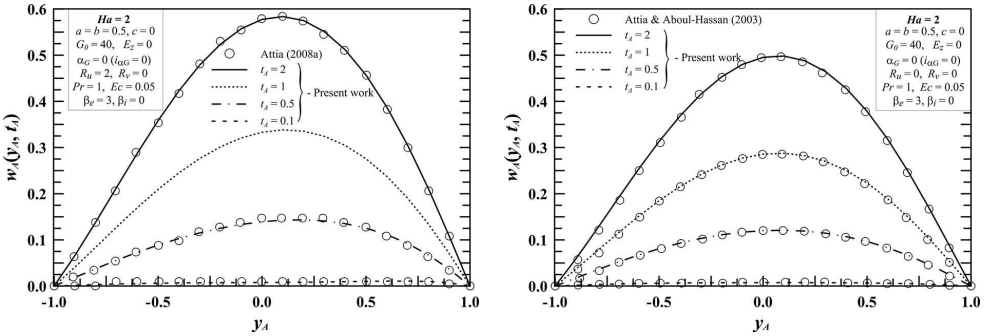

FIG. 3: Transversal velocity component profiles for the unsteady MHD: (a) Couette and (b) plane-Poiseuille flow at different times for Ha $= 2$

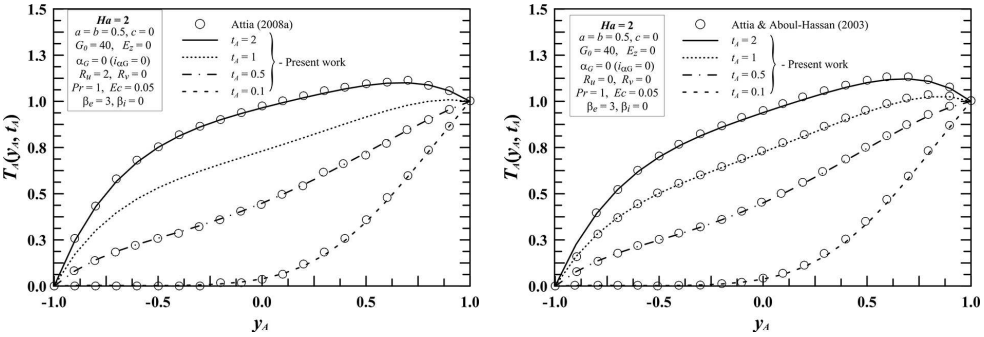

FIG. 4: Temperature profiles for the unsteady MHD: (a) Couette and (b) plane-Poiseuille flow at different times for Ha $= 2$

These figures, together with Figs. 2 and 3, clearly show the strong influence of the magnetic field on the velocity components. The overall effect of the Hartmann number on the flow field

is to flatten the velocity profiles, since the retarding Lorentz force increases with the Hartmann number. Despite that the effect of the Hartmann number (from Ha = 2 to 6) is to increase the Hall effects (reducing the axial component and increasing the transversal one), an elevated increase of the Hartmann number (from Ha = 6 to 10) can reduce the transversal velocity component, as illustrated in Figs. 5 and 6. These figures also point that at some instant of time the velocity profiles exceed their steady-state values, i.e., both the velocity profiles present an overshooting behavior with time evolution.

Figures 7, 8, and 9 illustrate the dynamics of the longitudinal and transversal velocity components, and temperature, respectively, at the center of the channel for different values of the Hall parameter, β_e, showing the relation of this parameter to the overshooting phenomenon. Figures 7(a), 8(a), and 9(a) refer to Ha = 6 and Figs. 7(b), 8(b), and 9(b) refer to Ha = 10. Comparisons are performed with the data of Attia and Aboul-Hassan (2003) and Attia (2005a) for plane-Poiseuille flow and for $G_o = 40$, $\alpha_G = 0$ ($i_{\alpha G} = 0$), $R_u = 0$, $R_v = 0$, Pr = 1, Ec = 0.05, $E_z = 0$, $a = 0.5$, $b = 0$, $c = 0$, and $\beta_i = 0$.

These figures reveal that the overshooting phenomenon is strongly related to large values of Hartmann and Hall parameters and, more than this, the steady-state regime is not monotonically

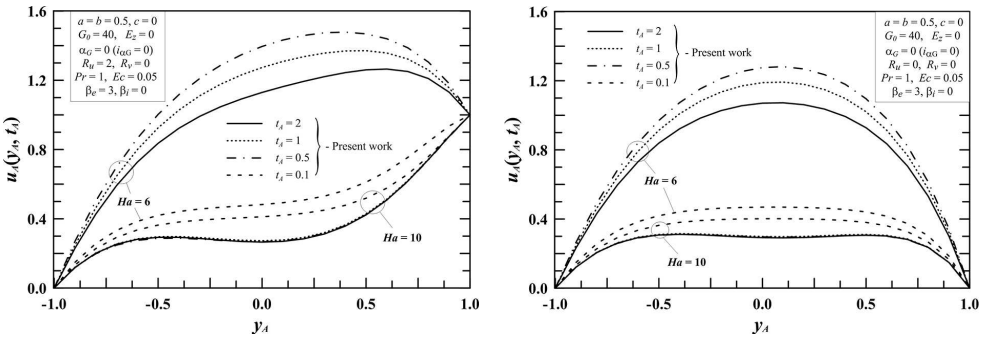

FIG. 5: Axial velocity component profiles for the unsteady MHD: (a) Couette and (b) plane-Poiseuille flow at different times for Ha = 6 and Ha = 10

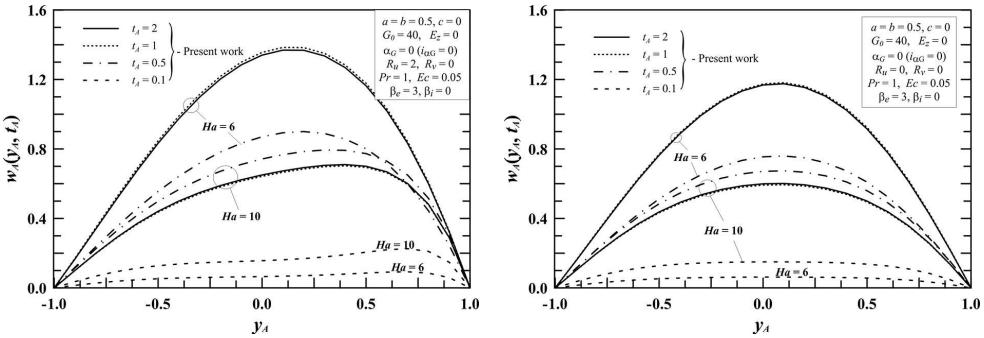

FIG. 6: Transversal velocity component profiles for the unsteady MHD: (a) Couette and (b) plane-Poiseuille flow at different times for Ha = 6 and Ha = 10

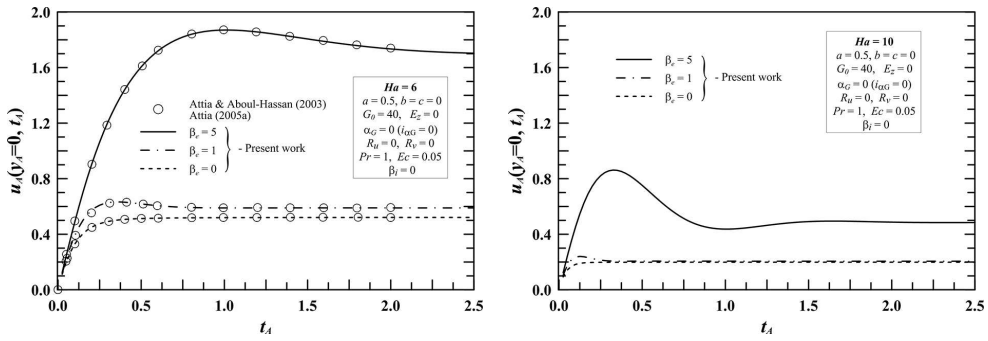

(a) (b)

FIG. 7: Evolution of the centerline axial velocity component for the unsteady Hartmann flow as function of the Hall parameter, β_e: (a) Ha $= 6$, (b) Ha $= 10$

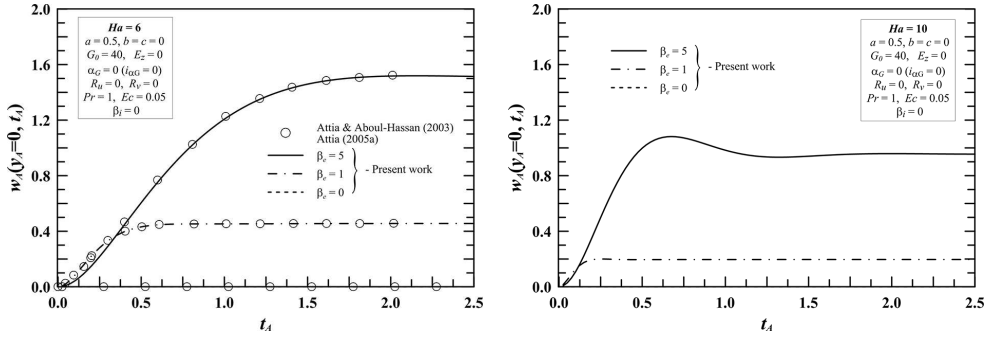

(a) (b)

FIG. 8: Evolution of the centerline transversal velocity component for the unsteady Hartmann flow as function of the Hall parameter, β_e: (a) Ha $= 6$, (b) Ha $= 10$

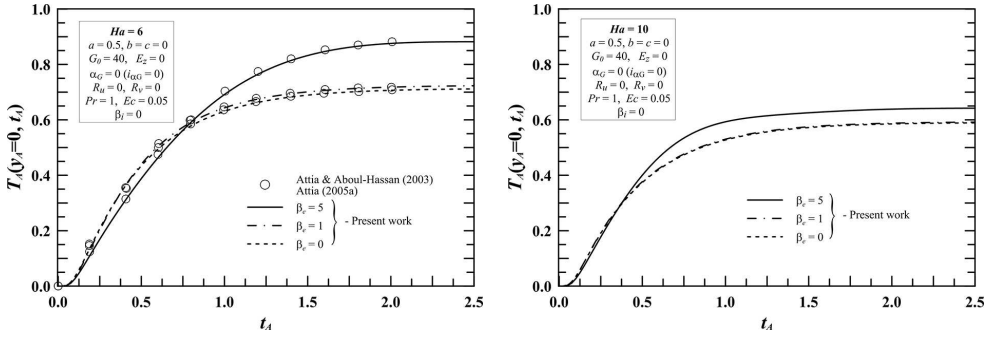

(a) (b)

FIG. 9: Evolution of the centerline temperature for the unsteady Hartmann flow as function of the Hall parameter, β_e: (a) Ha $= 6$, (b) Ha $= 10$

reached, i.e., the velocity profiles present an oscillatory-type behavior for small instants of time and then go to the terminal state. Although magnitude of the velocity components is more

attenuated, its occurrence is more evident for high Hartmann and Hall parameters. These figures also show that the time at which the longitudinal velocity component reaches its terminal steady-state regime increases with the Hall parameter, β_e. This is because this parameter governs the evolution of the transversal velocity component, which takes more time to develop, and as a consequence, the flow takes longer to arrive at the terminal state.

In addition to the overshooting phenomenon, another interesting behavior is revealed by Figs. 7 and 8 for small times. Although the Hall parameter, β_e, is the drive parameter for the transversal velocity component, w, at small times and for large values of β_e, an increasing in β_e produces a decrease in w. Attia and Aboul-Hassan (2003) and Attia (2005a) explain this behavior showing that at small times, w is very small, so that part of the source term related to the Hall effect of the transversal velocity can be approximated to $\beta_e u/(1+\beta_e^2)$, which decreases (and so does w) when increasing β_e. A similar behavior is also visualized in Fig. 9 for the centerline temperature evolution and the same analysis is extended for the source term relative to the Joule dissipation in the energy equation.

Now, Hall and ion-slip effects are simultaneously accounted and the present hybrid results are compared to the data of Attia (2003), who analyzed the steady Hartmann flow with heat transfer and variable viscosity, and to the findings of Attia (2006b), who considered the unsteady Hartmann flow with heat transfer within two porous plates under an exponential decaying pressure gradient and constant properties. Where not explicitly stated, the following values were employed for the dimensionless parameters: Ha $= 6$, $G_o = 40$, $R_u = 0$, Pr $= 1$, Ec $= 0.05$, $E_z = 0$, $a = 0$, $b = 0$, and $c = 0$.

Figures 10 to 12 show the effect of the Hall and the ion-slip parameters (β_e and β_i) on the steady-state longitudinal and transversal velocities and temperature profiles for $R_v = 0$ and $\alpha_G = 0$ ($i_{\alpha G} = 0$), and for two values of the Hartmann parameter (Ha $= 6$ and Ha $= 10$).

Except for the temperature profiles, the present results match the numerical ones of Attia (2003) for all values of Hall and ion-slip parameters analyzed. The differences between the results for the temperature field are attributed to a wrong mathematical description of the Joulean dissipation term in the energy equation in the work of Attia (2003) (the expression $(1+\beta_e\beta_i)$ should not be present in his mathematical formulation). This mistake is corrected later in the work of Attia (2006b), although there, the Joulean dissipation term was not multiplied by the Eckert parameter.

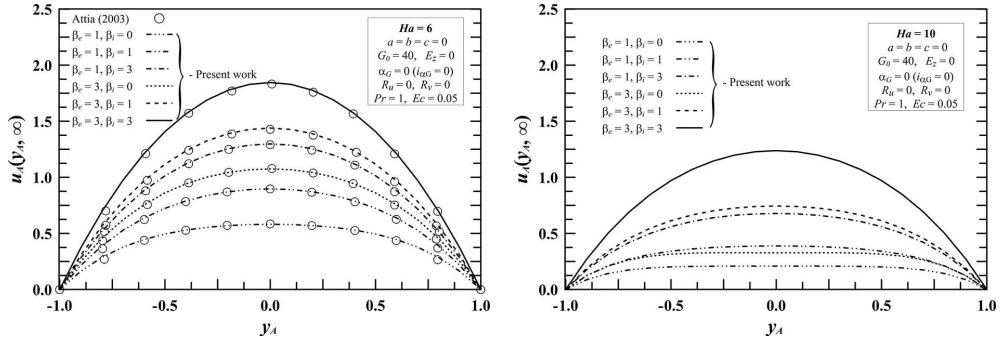

(a) (b)

FIG. 10: Axial velocity component profiles for the steady-state Hartmann flow as function of the Hall and ion-slip parameters, β_e and β_i: (a) Ha $= 6$, (b) Ha $= 10$

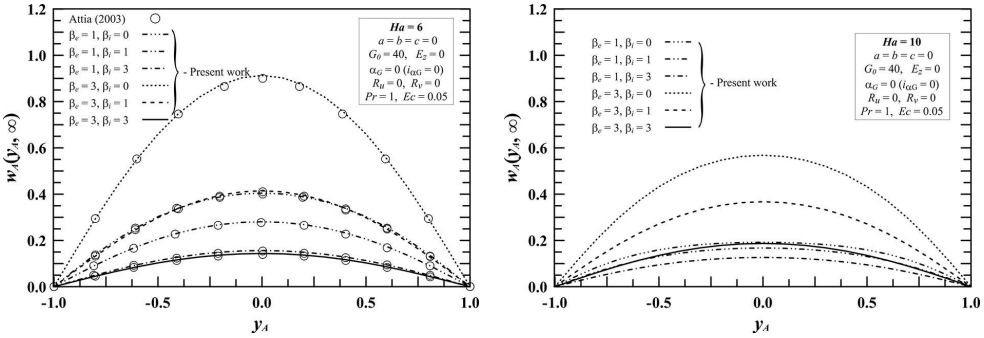

FIG. 11: Transversal velocity component profiles for the steady-state Hartmann flow as function of the Hall and ion-slip parameters, β_e and β_i: (a) Ha $= 6$, (b) Ha $= 10$

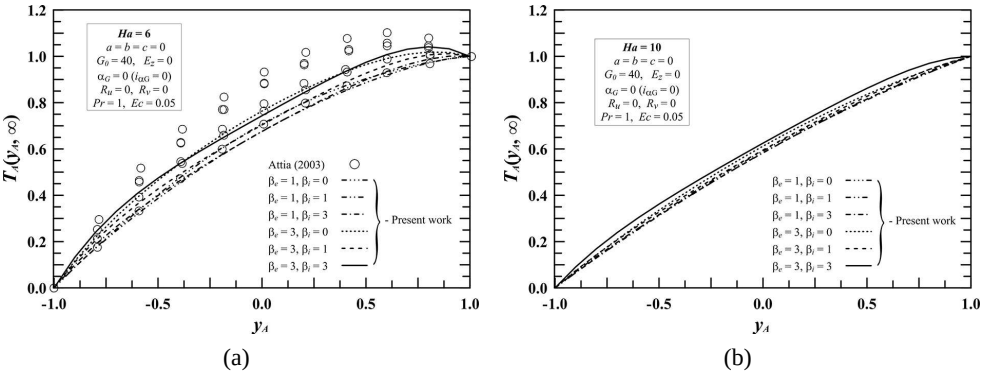

FIG. 12: Temperature profiles for the steady-state Hartmann flow as function of the Hall and ion-slip parameters, β_e and β_i: (a) Ha $= 6$, (b) Ha $= 10$

Regarding the influence of the Hartmann parameter on the flow and temperature fields under the presence of both Hall and ion-slip effects, these figures ratify the same trends of the retarding effect of the Lorentz force observed in the previous figures on the flow and temperature fields. In relation to the Hall and ion-slip effects on the flow field, figures show that increasing the Hall (β_e) or the ion-slip (β_i) parameters increases u. An increase in β_e or β_i reduces the electrical conductivity, and so the Lorentz retarding force on u. In general, increasing β_e increases the transversal velocity, w, since it is the result of the Hall effect. Increasing β_i produces a decrease in w, because this parameter decreases its source term and increases its damping term on the momentum equations (Attia, 2003).

Table 2 shows the results obtained with the present approach and illustrates some comparisons for the steady-state skin friction coefficients (longitudinal and transversal) and Nusselt number at both channel walls for different values of Hall and ion-slip parameters. Comparisons are performed with the results of Attia (2003).

Results clearly show the symmetry of the flow field through the opposite values of the axial and transversal skin friction coefficients at the top and bottom plates. An increasing in the ion-slip parameter (β_i) increases the magnitude of the axial skin-friction coefficient but decreases

TABLE 2: Steady-state skin-friction coefficients and Nusselt number for different values of β_e and β_i and Ha = 6, $G_o = 40$, $R_u = 0$, $R_v = 0$, Pr = 1, Ec = 0.05, $E_z = 0$, $a = 0$, $b = 0$, and $c = 0$

β_e	β_i	τ_{xA0}		τ_{xA1}		τ_{yA0}		τ_{yA1}	
		Present	**Attia (2003)**	**Present**	**Attia (2003)**	**Present**	**Attia (2003)**	**Present**	**Attia (2003)**
1	0	1.857	1.857	−1.857	−1.857	0.7308	0.732	−0.7308	−0.732
	0.5	2.142	2.385	−2.142	−2.385	0.5866	0.483	−0.5866	−0.483
	3	3.052	—	−3.052	—	0.2594	—	−0.2594	—
3	0	2.728	—	−2.728	—	1.509	—	−1.509	—
	0.5	3.022	—	−3.022	—	0.9857	—	−0.9857	—
	3	3.947	—	−3.947	—	0.2327	—	−0.2327	—
β_e	β_i	Nu_{A0}				Nu_{A1}			
		Present		**Attia (2003)**		**Present**		**Attia (2003)**	
1	0	0.9294		0.935		0.07061		0.065	
	0.5	0.9303		1.139		0.06973		−0.139	
	3	1.0873		—		−0.08728		—	
3	0	1.253		—		−0.2530		—	
	0.5	1.183		—		−0.1825		—	
	3	1.464		—		−0.4640		—	

the transversal one. In general, for low values of the Hall parameter, increasing the ion-slip parameter tends to decrease the magnitude of the Nusselt number, whereas for high values of (β_i) the Nusselt number behavior is not uniform anymore.

This table also reveals some small discrepancies between the hybrid results and those of Attia (2003). We believe the results presented by Attia (2003) are not fully converged. It is important to know that the present results, for the steady-state regime, were obtained from evolution of the unsteady-state situation. Then, to show that the present results are converged and that use of the filtering procedure by the integral transform method brings an additional advantage, Table 3 illustrates a convergence analysis for the skin-friction coefficient and Nusselt number for the situations for which comparisons with the results of Attia (2003) were performed.

The integral transform results for the skin friction are fully converged to four significant algorithms, and for the Nusselt number convergence to two significant digits is attained for the worst situation. The ability of the filtering procedure to automatically recover the steady-state solution for the flow field (requiring few or no number of terms) demonstrates the analytical nature and flexibility of the GITT approach. Since the filter employed for the temperature field is not representative of the steady-state regime, this table shows that a higher numbers of terms, especially for variable involving gradients, like the Nusselt number, is necessary.

Results for the unsteady Hartmann flow with heat transfer within two porous plates under an exponential decaying pressure gradient and Hall and ion-slip effects are now illustrated and compared with the findings of Attia (2006b). The following values were used for the dimensionless parameters: Ha = 6, $G_o = 40$, $R_u = 0$, $\alpha_G = 4$ ($i_{\alpha G} = 1$), Pr = 1, Ec = 0.05, $E_z = 0$, $a = 0$, $b = 0$, and $c = 0$.

TABLE 3: Convergence analysis for the steady-state skin-friction coefficients and Nusselt number for two cases analyzed in Table 2

β_e	β_i	N	τ_{xA0}	τ_{yA0}	Nu_{A0}	Nu_{A1}
1	0	10	1.857	0.7296	0.8995	0.1005
		50	1.857	0.7308	0.9240	0.07597
		100	1.857	0.7308	0.9272	0.07276
		200	1.857	0.7308	0.9289	0.07114
		300	1.857	0.7308	0.9294	0.07061
		Attia (2003)	1.857	0.732	0.935	0.065
	0.5	10	2.142	0.5858	0.8930	0.1070
		50	2.142	0.5866	0.9236	0.07638
		100	2.142	0.5866	0.9276	0.07239
		200	2.142	0.5866	0.9295	0.07040
		300	2.142	0.5866	0.9303	0.06973
		Attia (2003)	2.385	0.483	1.139	–0.139

Figure 13 illustrates the dynamics of the velocity components at the channel center for $R_v = 0$ and different combinations of the Hall and ion-slip parameters. Figure 14 brings the same evolution of these variables but now showing the influence of the wall porosity, $R_v \neq 0$, for $\beta_e = 3$ and different combinations of the wall suction/injection and ion-slip parameters (R_v and β_i).

Despite some differences between the present results and those obtained by Attia (2006b) the overall agreement is good. In order to show the accuracy of the main results obtained with the present approach, Table 4 brings a convergence analysis for the axial and transversal velocity components results shown in Figs. 13 and 14, at selected instants of time.

Evidently, very few terms are required to attain the convergence of the velocity components in the fourth significant digit. In fact, the transversal velocity component is already converged with only 10 terms in the expansion series for all instants of time illustrated. This table shows that only 50 terms are sufficient for convergence of all potentials. Results provided by Attia (2006b) certainly may be contaminated with some kind of numerical errors. In addition, since

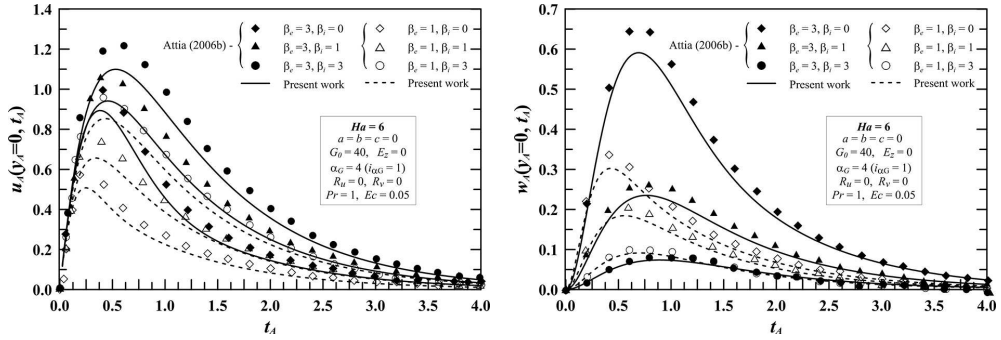

(a) (b)

FIG. 13: Evolution of the centerline (a) axial and (b) transversal velocity components as function of the Hall and ion-slip parameters, β_e and β_i, under a varying pressure gradient and non-porous walls

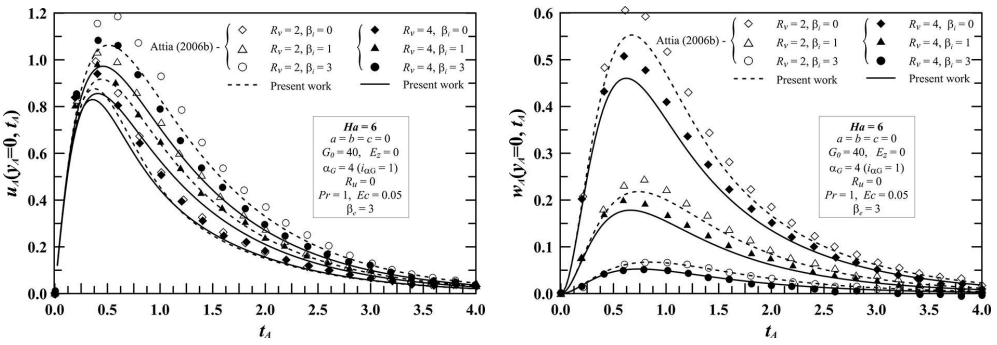

(a) (b)

FIG. 14: Evolution of the centerline (a) axial and (b) transversal velocity components as function of the Hall and ion-slip parameters, β_e and β_i, under a varying pressure gradient and porous walls

TABLE 4: Convergence of the centerline velocity components at select instants for different values of β_i and Ha $= 6$, $G_o = 40$, $R_u = 0$, $R_v = 0$, Pr $= 1$, Ec $= 0.05$, $\beta_e = 3$, $E_z = 0$, $a = b = c = 0$

N	$u_A\,(y_A = 0, t_A)$							
	$t_A = 0.25$		$t_A = 0.5$		$t_A = 1.0$		$t_A = 2.0$	
	$\beta_i = 0$	$\beta_i = 3$	$\beta_i = 0$	$\beta_i = 3$	$\beta_i = 0$	$\beta_i = 3$	$\beta_i = 0$	$\beta_i = 3$
10	0.8155	0.8812	0.8556	1.098	0.4574	0.8842	0.1455	0.3575
50	0.8146	0.8802	0.8549	1.098	0.4569	0.8837	0.1454	0.3573
100	0.8146	0.8802	0.8549	1.098	0.4569	0.8837	0.1454	0.3573
300	0.8146	0.8802	0.8549	1.098	0.4569	0.8837	0.1454	0.3573
	$w_A(y_A = 0, t_A)$							
10	0.2668	0.02566	0.5360	0.05716	0.5108	0.07302	0.1790	0.03782
50	0.2668	0.02566	0.5360	0.05716	0.5108	0.07302	0.1790	0.03782
100	0.2668	0.02566	0.5360	0.05716	0.5108	0.07302	0.1790	0.03782
300	0.2668	0.02566	0.5360	0.05716	0.5108	0.07302	0.1790	0.03782

Attia (2006) mistakenly did not include the Eckert number in the Joule heating term of the energy equation, results for the temperature field were not illustrated.

Regarding to computational costs, for $N < 50$ only few seconds are required to run the code, while for intermediary number of terms, $N = 100$, about 3 min are necessary. Above 100 terms, for example, for the highest number of terms in the series, $N = 300$, it took about 30 min to be executed in an Intel I5, 1.7 GHz computer with 4 GB of memory. If the adaptive procedure (Santos et al., 2001) had been employed, the time consumption would certainly be lower.

5. CONCLUSIONS

The outstanding potential of the integral transform method to handle problems where typical MHD coupling and non-linearity are present is demonstrated in the present work. One can

easily realize the interesting flexibility introduced by the filtering process, when simplified versions of the problem being solved are used, at first, to homogenize boundary conditions, but also to bring the additional gain of reducing the requirement of terms in the eigen-expansions in regions/instants where the filtering expression is representative, for example, the steady-state or fully developed region in channel flows. In these situations, for certain values of the dimensionless parameters, there is no need of additional series summation, once the solution is the analytical filtering function itself.

Convergence analyses clearly showed how very small terms in the series solution are required to provide results with excellent accuracy. Low time consuming is a characteristic of the GITT approach for small terms in the eigen-expansions.

A broad range of problems was handled with the present approach, starting with simple fully developed MHD Couette and plane-Poiseuille flows and then adding more interesting physical features like temperature-dependent transport properties, porous plates, Hall and ion-slip effects, and time-dependent pressure gradient.

Therefore, the unique hybrid characteristics demonstrated in the previous sections make the Generalized Integral Transform Technique an appropriate tool for benchmarking purposes in the field of magnetohydrodynamics, where strong current densities and body forces are responsible for modifications of the flow, temperature, and magnetic fields. Integral transform solutions of problems where flow induces internal magnetic fields and these, in its turn, modify the applied one (for high magnetic Reynolds numbers), are currently an object of research.

REFERENCES

Assad, G.E., *Hybrid Analysis of the Mutual Interaction Flow/Magnetic Fields in the Entrance Region of Parallel-Plate Channels*, MSc Thesis, Federal University of Paraíba, Brazil, 2016 (in Portuguese).

Attia, H.A., Transient MHD Flow and Heat Transfer between Two Parallel Plates with Temperature Dependent Viscosity, *Mech. Res. Commun.*, vol. **26**, no. 1, pp. 115–121, 1999. DOI: 10.1016/S0093-6413(98)00108-6

Attia, H.A., Unsteady MHD Flow and Heat Transfer of Dusty Fluid between Parallel Plates with Variable Physical Properties, *Appl. Math. Model.*, vol. **26**, no. 9, pp. 863–875, 2002. DOI: 10.1016/S0307-904X(02)00049-5

Attia, H.A., Steady Hartmann Flow with Temperature Dependent Viscosity and the Ion Slip, *Int. Commun. Heat Mass*, vol. **30**, no. 6, pp. 881–890, 2003. DOI: 10.1016/S0735-1933(03)00136-2

Attia, H.A., Magnetic Flow and Heat Transfer in a Rectangular Channel with Variable Viscosity, *Arab. J. Sci. Eng.*, vol. **30**, no. 2A, pp. 1–12, 2005a.

Attia, H.A., Unsteady Flow of a Dusty Conducting Fluid between Parallel Porous Plates with Temperature Dependent Viscosity, *Turk. J. Phys.*, vol. **29**, no. 4, pp. 257–267, 2005b.

Attia, H.A., Effect of the Ion Slip on the MHD Flow of a Dusty Fluid with Heat Transfer under Exponential Decaying Pressure Gradient, *Cent. Eur. J. Phys.*, vol. **3**, no. 4, pp. 484–507, 2005c. DOI: 10.2478/BF02475608

Attia, H.A., Steady MHD Couette Flow with Temperature-Dependent Physical Properties, *Arch. Appl. Mech.*, vol. **75**, nos. 4-5, pp. 268–274, 2006a. DOI: 10.1007/s00419-005-0420-7

Attia, H.A., Ion Slip Effect on Unsteady Hartmann Flow with Heat Transfer under Exponential Decaying Pressure Gradient, *Math. Probl. Eng.*, vol. 2006, Article ID 83937, 12 pages, 2006b. DOI: 10.1155/MPE/2006/83937

Attia, H.A., Unsteady MHD Couette Flow and Heat Transfer of Dusty Fluid with Variable Physical Properties, *Appl. Math. Comput.*, vol. **177**, no. 1, pp. 308–318, 2006c. DOI: 10.1016/j.amc.2005.11.010

Attia, H.A., The Effect of Variable Properties on the Unsteady Couette Flow with Heat Transfer Considering the Hall Effect, *Commun. Nonlinear Sci.*, vol. **13**, no. 8, pp. 1596–1604, 2008a. DOI: 10.1016/j.cnsns.2006.12.001

Attia, H.A., Unsteady Hydromagnetic Couette Flow of Dusty Fluid with Temperature Dependent Viscosity and Thermal Conductivity under Exponential Decaying Pressure Gradient, *Commun. Nonlinear Sci.*, vol. **13**, no. 6, pp. 1077–1088, 2008b. DOI: 10.1016/j.cnsns.2006.09.005

Attia, H.A. and Aboul-Hassan, A.L., The Effect of Variable Properties on Unsteady Hartmann Flow with Heat Transfer Considering the Hall Effect, *Appl. Math. Model.*, vol. **27**, no. 7, pp. 551–563, 2003. DOI: 10.1016/S0307-904X(03)00090-8

Attia, H.A. and Kotb, N.A., MHD Flow between Two Parallel Plates with Heat Transfer, *Acta Mech.*, vol. **117**, nos. 1-4, pp. 215–220, 1996. DOI: 10.1007/BF01181049

Attia, H.A., Abbas, W., and Abdeen, M.A.M., Ion Slip Effect on Unsteady Couette Flow of a Dusty Fluid in the Presence of Uniform Suction and Injection with Heat Transfer, *J. Braz. Soc. Mech. Sci. Eng.*, vol. **38**, no. 8, pp. 2381–2391, 2016. DOI: 10.1007/s40430-015-0311-y

Castelloes, F.V. and Cotta, R.M., Analysis of Transient and Periodic Convection in Microchannels via Integral Transforms, *Prog. Comput. Fluid Dyn.*, vol. **6**, no. 6, pp. 321–326, 2006. DOI: 10.1504/PCFD.2006.010772

Cotta, R.M., *Integral Transforms in Computational Heat and Fluid Flow*, Boca Raton, FL: CRC Press, 1993.

Cotta, R.M., Ed., *The Integral Transform Method in Thermal and Fluid Science and Engineering*, New York, NY: Begell House, 1998.

Cotta, R.M. and Mikhailov, M.D., *Heat Conduction: Lumped Analysis, Integral Transforms, Symbolic Computation*, Chichester, U.K.: John Wiley and Sons, 1997.

Cotta, R.M., Knupp, D.C., Naveira-Cotta, C.P., Sphaier, L.A., and Quaresma, J.N.N., Unified Integral Transforms Algorithm for Solving Multidimensional Nonlinear Convection-Diffusion Problems, *Numer. Heat Trans. A-Appl.*, vol. **63**, no. 11, pp. 840–866, 2013. DOI: 10.1080/10407782.2013.756763

Davidson, P.A., *An Introduction to Magnetohydrodynamics*, New York, NY: Cambridge University Press, 2001.

Hwang, C.L., Li, K.C., and Fan, L.T., Magnetohydrodynamic Channel Entrance Flow with Parabolic Velocity at the Entry, *Phys. Fluids*, vol. **9**, no. 6, pp. 1134–1140, 1966. DOI: 10.1063/1.1761812

IMSL Library, *Math/Lib*, Houston, TX: Visual Numerics Inc., 2010.

Lima, J.A., Quaresma, J.N.N., and Macêdo, E.N., Integral Transform Analysis of MHD Flow and Heat Transfer in Parallel-Plate Channels, *Int. Commun. Heat Mass*, vol. **34**, no. 4, pp. 420–431, 2007. DOI: 10.1016/j.icheatmasstransfer.2007.01.008

Lima, J.A. and Rêgo, M.G.O., On the Integral Transform Solution of Low-Magnetic MHD Flow and Heat Transfer in the Entrance Region of a Channel, *Int. J. Nonlinear Mech.*, vol. **50**, pp. 25–39, 2013. DOI: 10.1016/j.ijnonlinmec.2012.10.014

Matt, C.F.T., Quaresma, J.N.N., and Cotta, R.M., Analysis of Magnetohydrodynamic Natural Convection in Closed Cavities through Integral Transforms, *Int. J. Heat Mass Transfer*, vol. **113**, pp. 502–513, 2017. DOI: 10.1016/j.ijheatmasstransfer.2017.05.043

Mikhailov, M.D. and Ozisik, M.N., *Unified Analysis and Solutions of Heat and Mass Diffusion*, Toronto, Canada: Dover Publications, 1984.

Naveira, C.P., Lachi, M., Cotta, R.M., and Padet, J., Hybrid Formulation and Solution for Transient Conjugated Conduction-External Convection, *Int. J. Heat Mass Transfer*, vol. **52**, nos. 1-2, pp. 112–123, 2009. DOI: 10.1016/j.ijheatmasstransfer.2008.05.034

Ozisik, M.N. and Murray, R.L., On the Solution of Linear Diffusion Problems with Variable Boundary Condition Parameters, *J. Heat Transfer*, vol. **96**, no. 1, pp. 48–51, 1974. DOI: 10.1115/1.3450139

Pontes, F.A., Macêdo, E.N., Batista, C.S., Lima, J.A., and Quaresma, J.N.N., Hybrid Solutions Obtained via Integral Transforms for Magnetohydrodynamic Flow with Heat Transfer in Parallel-Plate Channels, *Int. J. Numer. Methods H.*, 2018. DOI: 10.1108/HFF-02-2017-0076

Santos, C.A.C., Quaresma, J.N.N., and Lima, J.A., Eds., Convective Heat Transfer in Ducts: The Integral Transform Approach, Rio de Janeiro, Brazil: E-Papers, 2001.

Setayesh, A. and Sahai, V., Heat Transfer in Developing Magnetohydrodynamic Poiseuille Flow and Variable Transport Properties, *Int. J. Heat Mass Transfer*, vol. **33**, no. 8, pp. 1711–1720, 1990. DOI: 10.1016/0017-9310(90)90026-Q

Shercliff, J.A., *A Textbook of Magnetohydrodynamics*, London, U.K.: Pergamon Press, 1965.

Shohet, J.L., Osterle, J.F., and Young, F.J., Velocity and Temperature Profiles for Laminar Magnetohydrodynamic Flow in the Entrance Region of a Plane Channel, *Phys. Fluids*, vol. **5**, no. 5, pp. 545–549, 1962. DOI: 10.1063/1.1706655

Sutton, G.W. and Sherman, A., *Engineering Magnetohydrodynamics*, New York, NY: Dover Publications, 2006.